

# Carbon monoxide emissions from the Washington, D.C. and Baltimore metropolitan area: Recent trend and COVID-19 anomaly

Israel Lopez-Coto,<sup>\*,†,‡</sup> Xinrong Ren,<sup>¶,§</sup> Anna Karion,<sup>†</sup> Kathryn McKain,<sup>||,⊥</sup> Colm Sweeney,<sup>||</sup> Russell R. Dickerson,<sup>¶</sup> Brian C. McDonald,<sup>#</sup> Doyeon Y. Ahn,<sup>¶</sup> Ross J. Salawitch,<sup>¶</sup> Hao He,<sup>¶</sup> Paul B. Shepson,<sup>@,‡</sup> and James R. Whetstone<sup>†</sup>

<sup>†</sup>*National Institute of Standards and Technology, 100 Bureau Dr, Gaithersburg, MD 20899*

<sup>‡</sup>*School of Marine and Atmospheric Sciences, Stony Brook University, 100 Nicolls Rd,  
Stony Brook, NY 11794*

<sup>1</sup> <sup>¶</sup>*Department of Atmospheric and Oceanic Science, University of Maryland, 4254 Stadium  
Dr, College Park, MD 20742*

<sup>§</sup>*Air Resources Laboratory, NOAA, 5830 University Research Court, College Park, MD  
20740*

<sup>||</sup>*NOAA Earth System Research Laboratory, Global Monitoring Laboratory, 325 Broadway,  
Boulder, CO 80305*

<sup>⊥</sup>*Cooperative Institute for Research in Environmental Sciences, University of Colorado,  
Boulder, CO 80309*

<sup>#</sup>*NOAA Earth System Research Laboratory, Chemical Sciences Laboratory, 325 Broadway,  
Boulder, CO 80305*

<sup>@</sup>*Department of Chemistry, Purdue University, 610 Purdue Mall, West Lafayette, IN 47907*

E-mail: israel.lopezcoto@nist.gov

## Abstract

We analyze airborne measurements of atmospheric CO concentration from 70 flights conducted over six years (2015-2020) using an inverse model to quantify the CO emissions from the Washington, DC and Baltimore metropolitan areas. We found that CO emissions have been declining in the area at a rate of  $\approx -4.5\%$  a<sup>-1</sup> since 2015, or  $\approx -3.1\%$  a<sup>-1</sup> since 2016. In addition, we found that CO emissions show a “Sunday” effect, with emissions being lower, on average, than for the rest of the week and that the seasonal cycle is no larger than 16 %. Our results also show that the trend derived from the NEI agrees well with the observed trend, but that NEI daytime-adjusted emissions are  $\approx 50\%$  larger than our estimated emissions. In 2020, measurements collected during the shutdown in activity related to the COVID-19 pandemic indicate a significant drop in CO emissions of 16 % relative to the expected emissions trend from the previous years, or 23 % relative to the mean of 2016 to February 2020. Our results also indicate a larger reduction in April than in May. Last, we show that this reduction in CO emissions was driven mainly by a reduction in traffic.

**Keywords:** Recent trend, Inverse modeling, Urban monitoring system, CO emissions, COVID-19

**Synopsis:** Experimental confirmation of a downward trend in CO emissions from the DC/Baltimore area and impacts induced by the COVID-19 pandemic response.

## Introduction

Carbon Monoxide (CO) is a toxic gas as well as a precursor of tropospheric ozone (O<sub>3</sub>) and carbon dioxide (CO<sub>2</sub>). CO is regulated by the EPA as a criteria air pollutant and its emissions have been declining in the United States (US)<sup>1-3</sup> and globally<sup>4-6</sup> for the last two decades, highlighting that more efficient combustion and emissions controls put in place by Federal and State Governments have been successful in reducing the emissions of this toxic gas and co-emitted air pollutants that contribute to ozone and fine particulate matter

(PM<sub>2.5</sub>).<sup>2,7</sup> In particular, previous work had showed a decreasing trend in CO concentrations in our area of interest using ground-level observations, and other measurements, from 1997 to 2010.<sup>3</sup>

Urban metropolitan areas are the main source of global air pollution given their high population densities, industrial activities, transportation systems and related emissions, including emissions of CO. In urban areas, CO is primarily formed by incomplete combustion of carbon-containing fuels, and mobile sources are the largest contributor to total CO emissions in the US.<sup>8</sup> In particular, for the Washington, D.C. and Baltimore, MD, census-defined metropolitan area, the on-road mobile sector represents 50 % of the total CO emissions while the total mobile sector (on-road + non-road) represents 88 % of the total CO emissions.<sup>8</sup>

In March 2020, the global response to the COVID-19 pandemic resulted in a dramatic decline in human activity across the world and, thus, a corresponding decline in pollutant emissions. Industrial activities, air travel, and road transportation were among the most affected sectors.<sup>9–11</sup> In particular, traffic counts from the area indicate traffic reductions of  $\approx 43$  % in April and  $\approx 27$  % in May for DC and Baltimore with respect to January 2020 (or  $\approx 50$  % in April and  $\approx 37$  % in May with respect to previous years) and fuel sales declined by  $\approx 44$  % in April and  $\approx 28$  % in May with respect to previous years (see Methods). However, quantifying such short-term reductions in CO emissions in 2020 caused by the pandemic response requires identification of the proper baseline, i.e., incorporating the predicted emissions from the long-term trend.

CO emissions in inventories are generally estimated based on emission models that combine activity data with emission factors.<sup>8,12–14</sup> However, atmospheric mole fraction measurements have also been successfully used to quantify CO emissions, greenhouse gases, and other pollutants using inverse data assimilation techniques. Researchers have used tower, satellite, and aircraft-based observations with transport models in an inversion framework to estimate trace gas emissions at regional,<sup>15–18</sup> urban,<sup>19–21</sup> and local scales.<sup>22</sup>

Here we use atmospheric CO measurements collected by research aircraft from 2015 to

2020 to estimate emissions in a Bayesian framework<sup>21</sup> to characterize the CO emissions phenomenology in the Washington DC and Baltimore metropolitan region. We quantify the absolute emissions, and temporal characteristics, in order to assess if CO emissions have continued to decline during the last years. In addition, measurements collected during the shutdown in human activities due to the COVID-19 pandemic response are used to estimate the impact of this anomaly on CO emissions.

## Methods

### Aircraft observations

Atmospheric CO mole fractions were observed from three instrumented aircraft for the period 2015 to 2020 as part of an ongoing long-term aircraft campaign that is part of the National Institute of Standards and Technology’s (NIST) North East Corridor (NEC) urban testbed<sup>21,23,24</sup> and as part of the East Coast Outflow (ECO) experiment.<sup>25</sup> A total of 70 flights (Fig. 1) were conducted, corresponding to 66 days across the 6-year period, mostly in winter and spring, with some flights in summer and fall. During the COVID shutdown, 15 of the 70 flights were conducted in 13 days from 16 April to 16 May 2020. The flights generally consisted of downwind transects at different altitudes that covered the full depth of the boundary layer, and at multiple distances from the cities of Washington, DC and Baltimore, MD, with at least one upwind transect to better characterize the upwind sources, and lasted between 3 to 4 hours during the afternoon. High-precision cavity ring-down spectrometers (CRDS), all calibrated to the WMO-CO-X2014A scale,<sup>26</sup> were used on board the aircraft to measure CO mole fractions at 0.4 Hz. The data were then averaged at 60 s resolution and the standard deviation for each minute calculated. Only data within the well-mixed boundary layer was kept for the inversion analysis. Typical measurement uncertainties estimated to be approximately 5 nmol mol<sup>-1</sup> (1- $\sigma$ ), determined by the instrument precision and drift as well as the uncertainties and drift of reference gases used in-flight calibrations

80 or pre-and-post flight calibrations on the ground. For all flights, reference gas data were  
81 calibrated on the WMO-CO-X2014A scale,<sup>26</sup> ensuring consistency in the measurements over  
82 multiple years within the uncertainty stated above. More details about the instrumentation  
83 and the aircraft can be found in Ren et al.<sup>27</sup> and in Plant et al.<sup>25</sup>

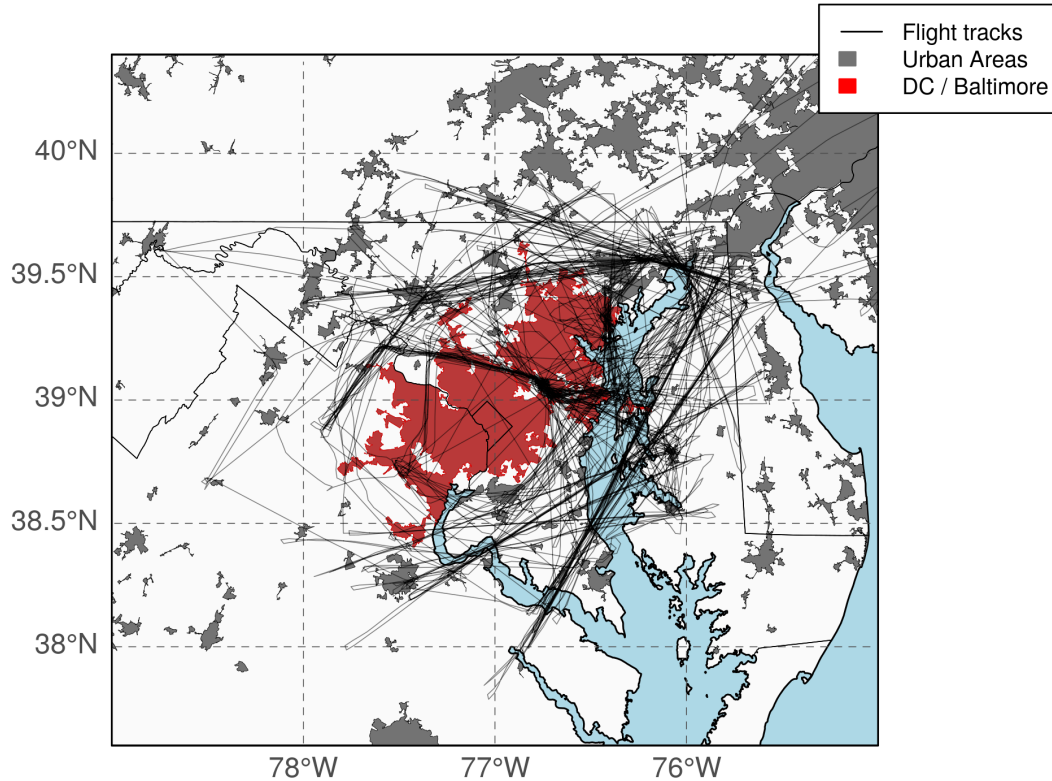


Figure 1: Flight tracks for all the flights and the DC/Baltimore region (red shaded area).

## 84 Transport model

85 Since the transit times in our modeling domain, and especially over the area of interest, are  
86 much smaller than the CO lifetime, we use a passive-tracer transport scheme. We use the  
87 Hybrid Single-Particle Lagrangian Integrated Trajectory (HYSPLIT) atmospheric transport  
88 and dispersion model<sup>28</sup> driven by two different meteorological models in order to character-  
89 ize the transport error and use the inter-model variance as a component of the model-data  
90 mismatch in the inversion. The first is the North American Mesoscale Forecast System

91 (NAM12)<sup>29</sup> generated by the National Center for Environmental Predictions (NCEP) and  
 92 provided by the National Oceanic Atmospheric Administration - Air Resources Laboratory  
 93 (NOAA-ARL), and the second is the European Center for Medium-Range Weather Fore-  
 94 casts (ECMWF) fifth-generation atmospheric reanalysis (ERA5)<sup>30</sup> provided by the Coper-  
 95 nicus Climate Change Service Climate Data Store (CDS).<sup>31</sup> NAM12 is provided with 26  
 96 vertical pressure levels, 12-km horizontal resolution and 3-hour temporal resolution. ERA5  
 97 is provided with 37 vertical pressure levels, 0.25° horizontal resolution and 1-hour tempo-  
 98 ral resolution. HYSPLIT was configured with the STILT vertical mixing and advection  
 99 schemes<sup>32,33</sup> and used the boundary layer heights from the meteorological models. 1000 par-  
 100 ticles were released for each 1-minute measurement along the flight tracks and tracked back  
 101 in time for 48 h with a model time step of 1 min. Then, influence functions, or footprints,  
 102 representing each observation's sensitivity to surface emissions<sup>32</sup> were calculated at 0.1° and  
 103 0.03° spatial resolution.

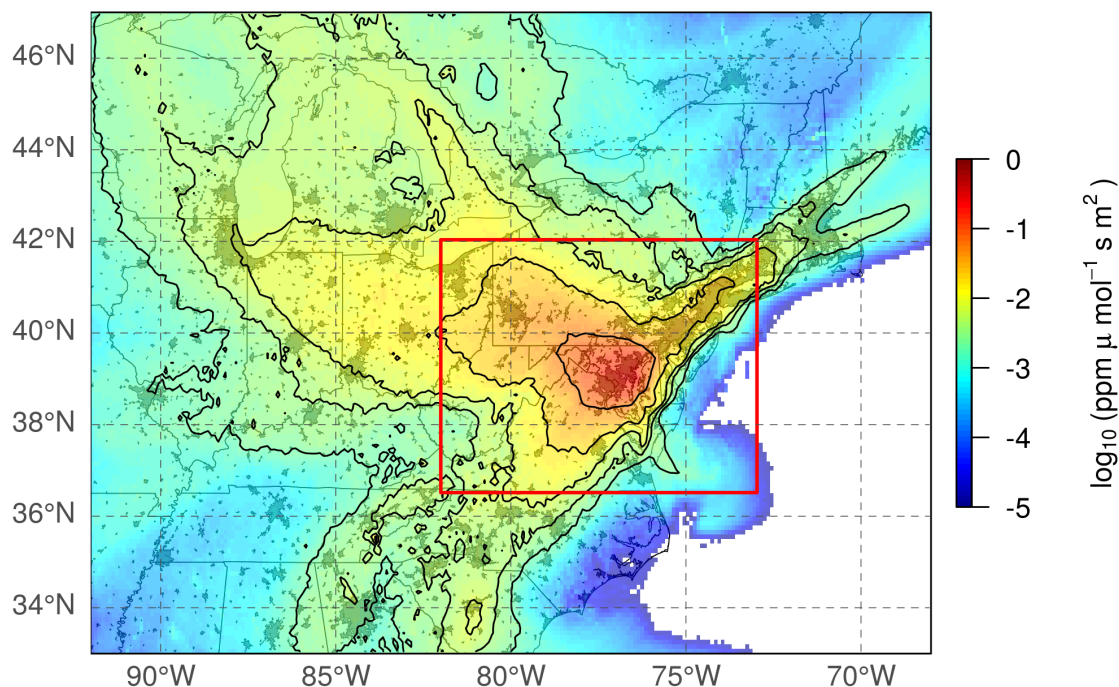


Figure 2: Cumulative footprint, or influence function, representing the measurements’ sensitivity to surface emissions, averaged across flights (note the logarithmic color-scale). Nested domains used in the inversion are also shown with the full extent of the figure being the large, coarser resolution domain and the red square depicting the extent of the smaller, higher resolution domain. Black contours show (from the inside out) the 99<sup>th</sup>, 95<sup>th</sup>, 85<sup>th</sup>, 70<sup>th</sup> and 50<sup>th</sup> quantiles of the footprint. Urban areas and state borders are also shown in grey.

## Tiered Multi-Resolution Inverse Modeling Approach

Similarly to Lopez-Coto et al.,<sup>21</sup> we estimated trace gas emissions using a Bayesian inverse framework. However, in this work, we implemented a tiered multi-resolution inverse modeling approach, consisting of a two-step sequential Bayesian inversion based on the ideas of Rödenbeck et al.;<sup>34</sup> but using the same transport model in both steps, although at different resolutions. We first estimate the emissions (CO emissions in this work) in a coarse (0.1°), large domain (Figure 2) so that upwind sources are optimized. Then, we use the optimized emissions from the first inversion to estimate the contribution of the upwind sources in the background of the smaller, higher-resolution (0.03°) domain and then proceed with the

113 higher-resolution inversion.

114 Each inversion step solves the classical Bayesian inverse problem for each flight, where  
115 optimum posterior estimates of fluxes are obtained by minimizing the cost function  $J$ :<sup>35,36</sup>

$$J(\mathbf{x}) = \frac{1}{2} \left[ (\mathbf{x} - \mathbf{x}_b)^T \mathbf{P}_b^{-1} (\mathbf{x} - \mathbf{x}_b) + (\mathbf{H}\mathbf{x} - \mathbf{y})^T \mathbf{R}^{-1} (\mathbf{H}\mathbf{x} - \mathbf{y}) \right] \quad (1)$$

116 where  $\mathbf{x}_b$  is the first guess or *a priori* (prior) state vector,  $\mathbf{P}_b$  the *a priori* error covariance  
117 matrix which represents the uncertainties in our *a priori* knowledge about the fluxes and  $\mathbf{R}$   
118 the error covariance matrix, which represents the uncertainties in the observation operator  
119  $\mathbf{H}$  and the observations  $\mathbf{y}$ , also known as model-data mismatch. The state vector in our  
120 setup is composed only of fluxes, and the prior fluxes ( $\mathbf{x}_b$ ) are taken from a bottom-up  
121 inventory described later. The observation operator  $\mathbf{H}$  is constructed using the sensitivity  
122 of observations to surface fluxes, or footprints (units: ppm  $\mu\text{mol}^{-1} \text{ m}^2 \text{ s}$ ) generated by the  
123 transport model (HYSPLIT).

124 Here,  $\mathbf{x}_b$  is taken as constant in time and, thus, a single exponential covariance model<sup>37</sup>  
125 for  $\mathbf{P}_b$  is chosen to account for spatial correlations. 100 % of the prior grid cell emissions is  
126 used as prior flux uncertainty to account for the large reported uncertainties in inventories at  
127 this level<sup>38,39</sup> as well as the lower representativity of the prior at the daily scale arising from  
128 the fact that we intentionally choose to use an average prior for a fixed year for the whole  
129 period. A lower limit of 1 nmol  $\text{m}^{-2} \text{ s}^{-1}$  was set for the flux uncertainty. The correlation  
130 length (L) was set at 10 km as in previous work<sup>21,23</sup>

131 For  $\mathbf{R}$ , a double exponential covariance model<sup>40</sup> is used. Diagonal terms are computed  
132 as the 1-min variance in the measurements, the background variance and the inter-model  
133 variance of the transport models ensemble.<sup>21,41,42</sup> A lower limit of  $(5 \text{ nmol mol}^{-1})^2$  was also  
134 used for the total variance. A correlation length (L) of 1 km and time-scale ( $\tau$ ) of 1 h were  
135 used since short characteristic length and time scales have been shown for atmospheric trace  
136 gases in urban environments.<sup>43,44</sup>



## Background estimation

We define the “long-range” background as the molar fraction of trace gas in the air flowing into the large domain (Fig. 2) for a particular flight. Because our measurements do not reach the boundaries of the domain, we first determine a “measured background” as the 5<sup>th</sup> percentile of the observed values. However, this “measured background” also includes the contribution from sources within the domain (“inside contribution”) which we approximate as the 5<sup>th</sup> percentile of the ensemble of transport models mean of simulated enhancements. Thus, the “long-range” molar fraction is approximated by subtracting the “inside-contribution” from the “measured-background”.

For the second, high-resolution inversion, in addition to the previously computed “long-range” background, the contribution of the nearby outside sources (sources within the large domain but not in the **nested** domain) is incorporated into the background using the optimized fluxes from the coarser domain inversion posterior. This step helps to better characterize the outside contribution by using upwind sources already optimized as opposed to relying on the prior.

## Bottom-up emissions

As the inversion prior ( $\mathbf{x}_b$ ), we use the fuel-based CO emissions inventory of motor-vehicle emissions (FIVE),<sup>12,14</sup> provided at 12-km and 4-km resolution for July 2018 (These emission files were created for the Long Island Sound Tropospheric Ozone Study (LISTOS) and New York Investigations of Consumer Emissions (NYICE) in 2018, and can be found at.<sup>45</sup> FIVE replaces the whole "on-road" and "non-road" sectors of the NEI-2014 but maintains the rest of sectors. The fluxes are reprojected using a bilinear interpolation method to 0.1° and 0.03° respectively for each domain used in the tiered inversion. We use the weekday, daytime hours (09:00 to 18:00 EST) average as prior emissions, constant in time, in the inversion consistently for the whole period. The prior emissions are kept constant among inversion days so that temporal changes in the posterior are not a consequence of changes in the prior

emissions.

We use annual CO emissions estimates reported<sup>46</sup> by the EPA in the NEI to compare with our posterior emissions estimates. The EPA estimates are at state level. However, our study area (red, Fig. 1 ) contains three states (Maryland, Virginia, and the District of Columbia) and thus we account for the proportion of each state’s total emissions that originate in the part of the urban area that belongs to each of the three states using the FIVE spatial distribution. This results in a weighted annual CO emissions estimate for our accounting area composed of 22 % of Virginia (VA) emissions, 56 % of Maryland (MD) emissions and 100 % of District of Columbia (DC) emissions. In addition, since our aircraft measurements were conducted during afternoon hours, the inversion results represent daytime emissions ( $\approx$  09:00 to 18:00 EST) rather than a 24 h average and, thus, to compare them with the NEI bottom-up estimates in a consistent way, the FIVE’s daily cycle is applied to the EPA’s annual emissions. This results in emissions  $\approx$  50 % larger than the reported annual mean.

Last, to estimate the impact of COVID-related traffic reductions on CO emissions we use four activity proxies. The first two are directly derived from traffic counts and, as such, are a measure of how traffic changed. The first one measures the traffic counts<sup>47–49</sup> changes during 2020 from 127 stations in DC and Baltimore with respect to the first three weeks of 2020, while the second measures the changes in traffic counts with respect to the 2018 and 2019 weekly average for the same stations. In addition, we use the Apple mobility index<sup>50</sup> data for DC/Baltimore area, which is a proprietary index published by Apple Inc. during the pandemic that attempts to quantify the “mobility” using cellphone data. Last, we consider the declines in monthly “motor gasoline” fuel sales,<sup>51–53</sup> using as reference the 2018 and 2019 monthly average (Fig. 3). State fuel totals are combined using the same proportions presented in the previous paragraph. All these activity reduction proxies are then combined with the relative fraction of total emissions produced by, i) mobile on-road ( $\approx$  50 %) and, ii) mobile on-road + non-road ( $\approx$  88 %) sectors from the NEI-2017<sup>8</sup> to produce relative CO emissions reductions. Then, they are averaged (for the appropriate days) to calculate the

average reduction for the months of April and May for these two sectors independently. The standard deviation is also calculated among the different proxies and dates.

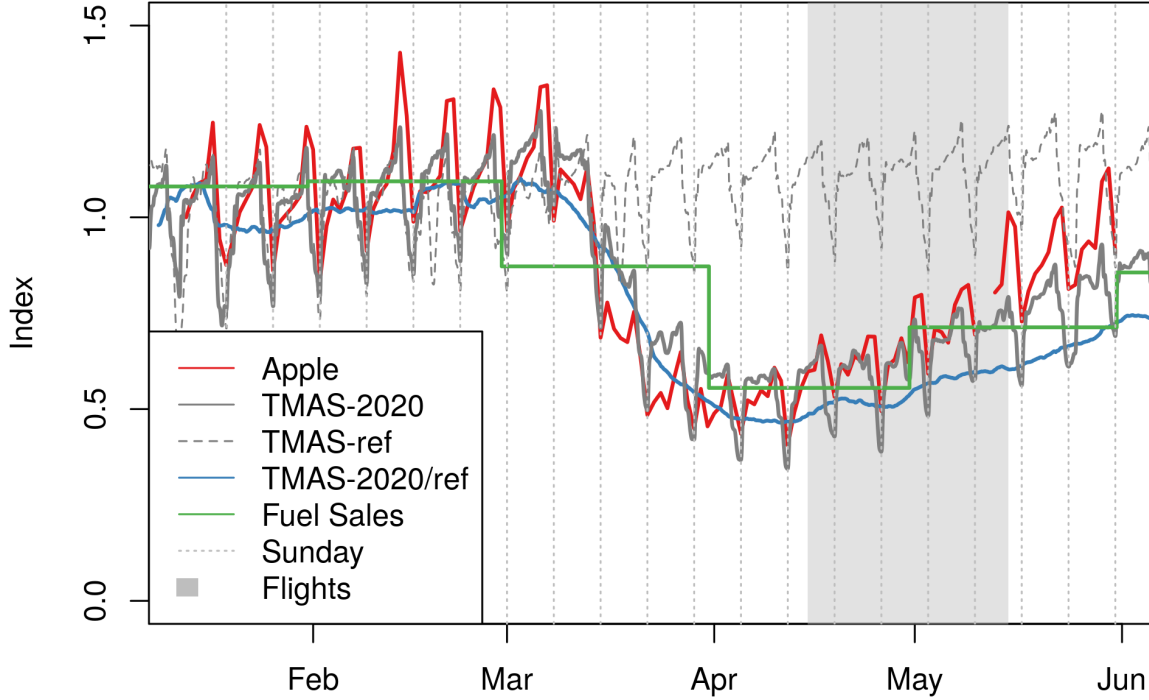


Figure 3: Comparison of the time-series for the Apple daily mobility index for DC/Baltimore area (red), traffic counts during 2020 for 127 stations in DC and Baltimore normalized to the first three weeks of 2020 (TMA2020, grey solid line), 2018 and 2019 averaged traffic counts for the same stations (TMAref, grey dashed line), traffic counts reduction in 2020 with respect to the 2018 and 2019 weekly averages, (TMA2020/ref, blue), and “motor gasoline” fuel sales declines from the 2018 and 2019 monthly average (green). Sundays and period when the flights happened during the lock-downs are also shown. Note that the TMAref series has been shifted to match the day of the week in 2020. (TMA: Travel Monitoring Analysis System).

## Results

### Emission Rates

CO emission rates for the Washington, DC - Baltimore, MD area were estimated using an inverse modeling technique<sup>21</sup> with aircraft measurements collected over 6 years (2015 to 2020). Figure 4 shows the posterior CO emission rates estimated by the atmospheric

inversion for the DC/Baltimore area (red area in Fig. 1) grouped by a) year, b) month, and  
 c) day of the week. Each group (box and whiskers) contains all individual estimates from  
 inverse calculations using two different transport models, and for each of N flights included in  
 the group. The dominant source of variability in posterior emissions was the daily variability,  
 $\approx 32\%$ , which, as discussed in previous work, represents a combination of real variability in  
 emissions and methodological uncertainty.<sup>21</sup> In particular, the median spread in the posterior  
 emissions due to the transport model for any particular day was about  $\approx 8\%$ , which imposes  
 a limit to the detectability of changes in daily emissions. However, at longer time scales, the  
 median variability due to the transport model for each annual campaign (from 5 to 16 flights  
 per year in this work) was just  $\approx 3.8\%$ . This indicates that the addition of flight days can  
 partially mitigate the transport model uncertainty and increase our ability to detect smaller  
 changes in emissions at these longer temporal scales. The annual variability is approximately  
 $15\%$ , very similar to the monthly variability,  $14\%$ , and weekday variability,  $16\%$  (all defined  
 as  $1-\sigma$  of the means). However, it is clear that 2015 and 2020 stand out for having higher,  
 and lower emissions, respectively, than the average for the period from 2016 to 2019 (Fig.  
 4a). In fact, the annual variability between 2016 and 2019 is just  $8\%$  while the monthly  
 variability remains about the same ( $16\%$ ). The monthly emissions (Fig. 4b) do not show  
 any apparent seasonal cycle outside the range of the monthly variability. Nevertheless, the  
 number of flights for some of the months is small and thus the mean estimates are more  
 uncertain. As a point of comparison, fuel sales and traffic counts show a seasonal cycle of  
 $\approx 5\%$  indicating that more flights will be needed during summer months to uncover the  
 presence of any seasonal pattern in CO emissions. Sunday emissions are lower than weekday  
 emissions (Fig. 4c) reflecting reduced traffic and industrial activities on Sundays, as also  
 shown by the traffic counts and mobility index (Fig. 3). Our results for CO emissions show  
 that the average for the period from 2016 to 2019 agrees well with the daytime emissions  
 from the FIVE inventory (used as prior), as also shown in previous work.<sup>14</sup> In addition,  
 CO emissions in February 2016 match, within 1 standard deviation, those estimated in a

previous analysis,<sup>21</sup> in which a larger number of transport models and prior inventories were used and a large sensitivity analysis was conducted, providing additional confidence in our current estimated emissions.

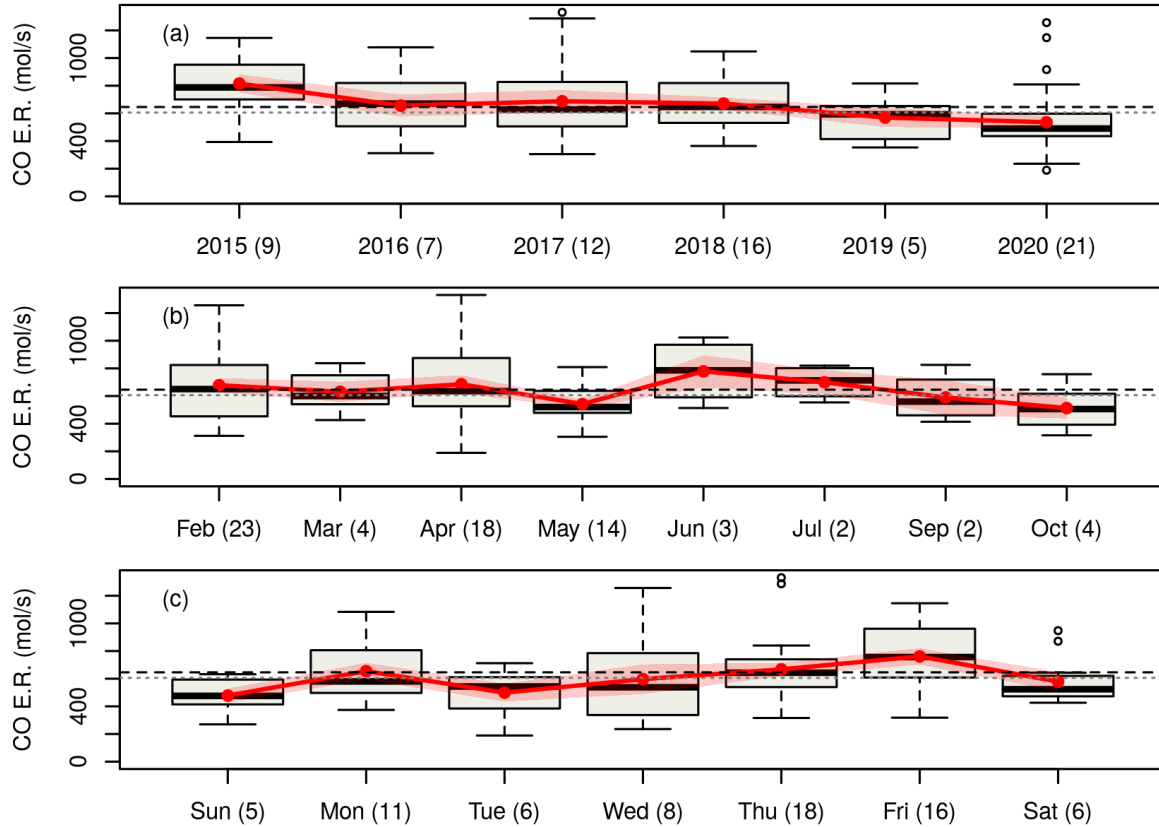


Figure 4: Boxplots of CO posterior estimated emission rates (E.R.) for DC/Baltimore grouped by a) year, b) month and c) day of the week. Boxes indicate the the inter-quartile range (IQR), i.e. the 25<sup>th</sup> to 75<sup>th</sup> percentile range, whiskers the range up to 1.5 times the IQR, circles the outliers ( $> 1.5 \times \text{IQR}$ ) and the black line the median. The black dashed line represents the average emission rate for the period 2016 to 2019. The grey dotted line represents the emission rate of the daytime FIVE inventory, used as the prior. The red, solid circles connected with the red line represent the mean top-down estimate and the red shaded area represents the standard error of the mean. The number of flights per group is shown in parentheses.

The spatial distribution of the posterior emissions averaged by year is shown in Figure 5. Clear patterns associated with urban emissions, including traffic, seem to dominate as expected. Also, changes among years are evident, showing for example the overall higher emissions in 2015 or lower emissions in 2020, but without dramatic spatial differences. This

231 result is however expected as most of the emissions sources are in the same locations.

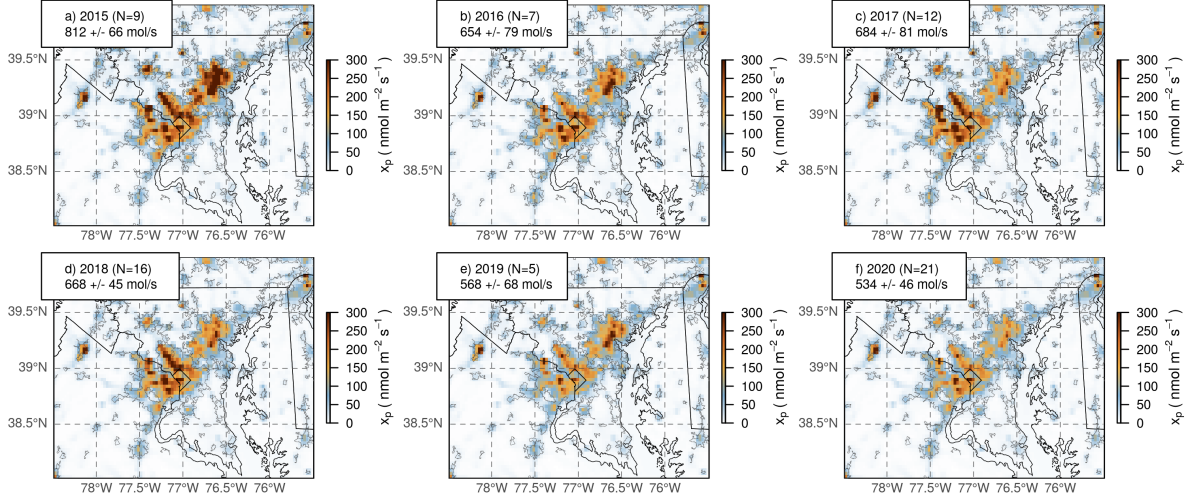


Figure 5: CO posterior flux ( $x_p$ ) averaged by year. The number of flights (N) and the mean total emission rate  $\pm$  the standard error for each year are indicated in each panel. Color-scale is saturated at the maximum value shown.

## 232 Trends and Anomaly Detection

233 According to EPA’s state-level National Emissions Inventory (NEI), CO emission rates  
 234 (daytime-adjusted and spatially allocated to the Washington, DC and Baltimore metropoli-  
 235 tan area, see Methods) declined at a rate of  $(-150 \pm 6) \text{ mol s}^{-1} \text{ a}^{-1}$  (1- $\sigma$  and thereafter)  
 236 between 1996 and 2010, with a smaller but still significant trend of  $(-32 \pm 6) \text{ mol s}^{-1} \text{ a}^{-1}$   
 237 from 2011 to 2019. However, for the period from 2016 to 2019 the trend was even smaller  
 238 with just  $(-17 \pm 4) \text{ mol s}^{-1} \text{ a}^{-1}$ , Table 1. The sharp decrease in CO during the 1990s is  
 239 attributed to the universal adoption of port fuel injection, the elimination of carburetors and  
 240 the success of three-way catalytic converters in controlling tailpipe emissions, including co-  
 241 emitted volatile organic compounds (VOCs) that contribute to secondary ozone and aerosol  
 242 formation.<sup>2,54</sup> More recently, there are expected diminishing CO reductions from emission  
 243 control technologies implemented on automobiles over many decades.<sup>55,56</sup>

244 Figure 6 shows a comparison of the yearly averaged posterior emission rates (i.e., atmo-  
 245 spheric measurement based, or top-down, estimates<sup>57</sup>) and the bottom-up estimates derived

Table 1: CO emissions trend ( $\text{mol s}^{-1} \text{ a}^{-1}$ ) for the DC/Baltimore urban area for different periods calculated using the measurements (top-down) and derived from the daytime-adjusted NEI reported values (bottom-up). p-values in brackets. (\*pre-COVID).

| Period     | Top-down             | Bottom-up                  |
|------------|----------------------|----------------------------|
| 1996-2010  | N.A.                 | $-150 \pm 6$ ( $<<0.001$ ) |
| 2011-2019  | N.A.                 | $-32 \pm 6$ (0.001)        |
| 2015-2020* | $-37 \pm 13$ (0.044) | $-44 \pm 15$ (0.066)       |
| 2016-2020* | $-20 \pm 13$ (0.21)  | $-17 \pm 4$ (0.048)        |

from the NEI for the area of interest. As discussed before, top-down estimated emissions in 2015 are larger than the average between 2016 and 2019, which is also shown by the bottom-up estimates. On the other hand, the bottom-up daytime-adjusted emissions ( $\approx 09:00$  to  $18:00$  EST time) are  $\approx 50$  % larger than the inversion posterior estimates.

The annual trend obtained with the inversion for the period 2016 to 2020 (before the COVID lock-down) is  $(-20 \pm 13) \text{ mol s}^{-1} \text{ a}^{-1}$  (p-value = 0.21). This trend is similar to, although slightly larger than, the trend obtained from the daytime-adjusted EPA estimates ( $(-17 \pm 4) \text{ mol s}^{-1} \text{ a}^{-1}$ , p-value = 0.048). The EPA trend is within the uncertainty of the posterior estimate trend, making them indistinguishable. However, due to the larger uncertainty obtained in our top-down estimates, we cannot establish our measured trend as statistically significant.

Including 2015 in the trend estimation, our top-down trend becomes  $(-37 \pm 13) \text{ mol s}^{-1} \text{ a}^{-1}$ . This trend is 2.8 times the associated uncertainty, with a p-value of 0.044, and is larger than for the period from 2016 to 2020. However, the relative uncertainty is smaller, 35 %, as compared to the previous 65 %, and the p-value smaller, being now statistically significant at the 95 % level. On the other hand, the bottom-up trend is  $(-44 \pm 15) \text{ mol s}^{-1} \text{ a}^{-1}$  with a p-value of 0.066. As with the top-down case, this trend is larger, but is more uncertain and is no longer statistically significant at the 95 % level.

As mentioned in the previous section, the 2020 top-down emissions estimates for CO were lower than in previous years (Figure 4a). However, by separating the 2020 estimations made before (February 2020) and during the COVID-19 induced lock-down (16/04/2020

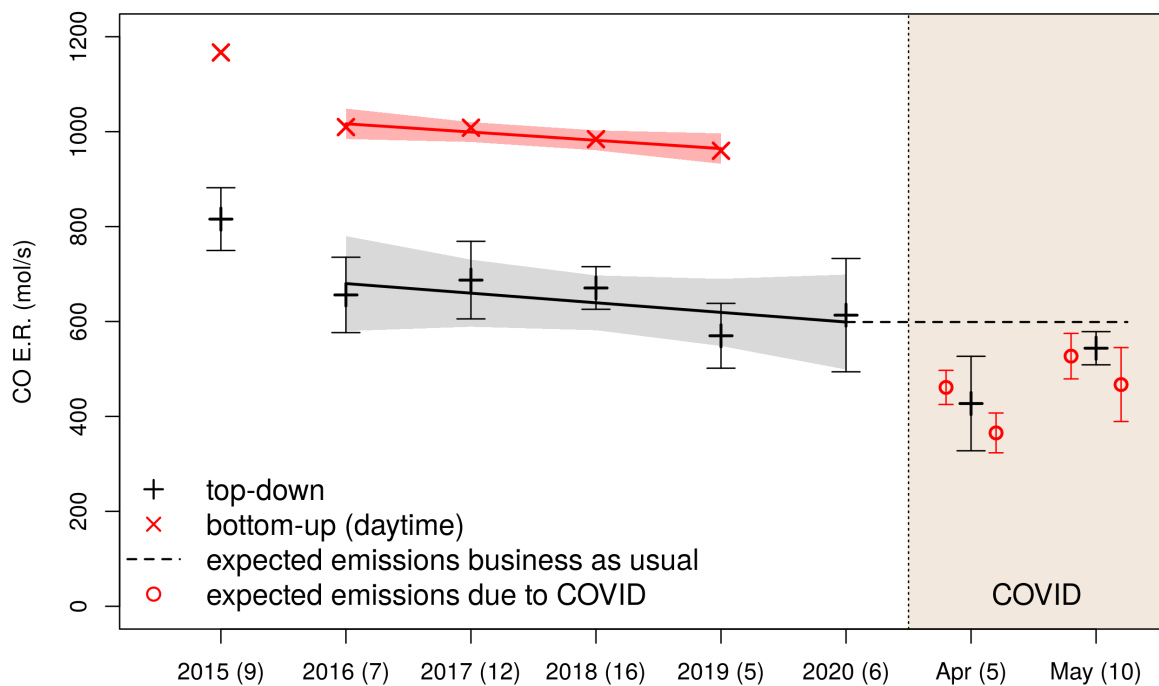


Figure 6: CO posterior (top-down) emissions rates for DC/Baltimore by year compared to EPA bottom-up estimates (scaled-up to represent daytime values) and annual trends. Shaded areas indicate the 95 % confidence interval of the corresponding trendlines between 2016 and 2020 (top-down; 2020 estimate calculated without the COVID-affected flights) and 2016 and 2019 (bottom-up). Errors bars indicate the standard error of the posterior annual means. The COVID period is also shown separated between 16 - 30 April 2020 and 1 - 16 May 2020. The dashed line represents the expected emissions for 2020 extrapolated from the top-down trend and the red circles are expected emissions after accounting for mobile sector reductions (on-road only and on-road+non-road) due to mobility changes during the COVID lock-down using the extrapolated top-down trend as reference. Error bars (red) in the COVID extrapolations represent the 1- $\sigma$  daily variability within the month. The number of flights in each group is given in parentheses.



267 to 16/05/2020), (Figure 6), it is clear that emissions during the lock-down period were  
 268 lower on average. Specifically, we see a 16 % ( $(96 \pm 51)$  mol s<sup>-1</sup>) reduction with respect  
 269 to the expected 2020 emissions using the calculated top-down linear trend (dashed line),  
 270 or 23 % ( $(149 \pm 54)$  mol s<sup>-1</sup>) with respect to the averaged top-down value for the period  
 271 2016 to February 2020. These reductions for the lock-down period relative to either the  
 272 long-term trend or the mean of previous years are more than 1.9 or 2.8 times the standard  
 273 error of the observed difference, respectively. In April, the emissions were reduced 28 %  
 274 ( $(171 \pm 104)$  mol s<sup>-1</sup>) with respect to the expected 2020 emissions using the calculated top-  
 275 down linear trend, or 34 % ( $(219 \pm 105)$  mol s<sup>-1</sup>) with respect to the averaged top-down  
 276 value for 2016 to February 2020. In May, the reduction was smaller, 9 % ( $(55 \pm 45)$  mol s<sup>-1</sup>)  
 277 using the top-down linear trend or 16 % ( $(102 \pm 48)$  mol s<sup>-1</sup>) with respect to the 2016 to  
 278 February 2020 averaged. Our CO emissions declines are consistent with expected reductions  
 279 in traffic emissions (Figure 6) estimated using traffic counts, fuel sales and mobility metrics  
 280 (see Methods), as well as sectoral attribution provided by the NEI, further indicating that  
 281 traffic was the main driver for the observed CO emissions decline and that it was substantially  
 282 reduced in April relative to previous years, but then rebounded in May as the populations  
 283 in these cities relaxed restrictions on activity.

284 The spatial distribution of emissions for the pre-COVID period (excluding the high-  
 285 emissions year 2015) along with the emissions map during the COVID shutdown and the  
 286 differences between them are shown in Figure 7. The largest absolute reductions are mostly  
 287 seen where emissions were the largest in the pre-COVID period, with a general reduction of  
 288 emissions in the urban areas. We can also estimate the relative reduction in the two separate  
 289 metropolitan areas, resulting in a  $\approx 26$  % average relative reduction for the Baltimore, MD,  
 290 census-designated area and an  $\approx 18$  % average relative reduction for the Washington, DC–  
 291 VA–MD, census-designated area. However, due to the larger uncertainty for the reduction  
 292 ratios at these smaller spatial scales, these differences between cities are not statistically  
 293 significant.

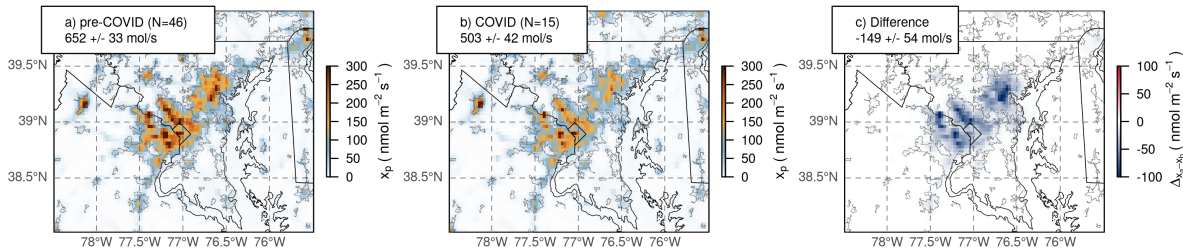


Figure 7: CO posterior emissions maps averaged a) between 2016 and February 2020, representing a pre-COVID estimate, b) during the COVID lock-down (16/04/2020 to 16/05/2020) and c) spatial differences between the two. The number of flights (N) and the mean total emissions  $\pm$  the standard error for each are indicated in each panel.

## Implications

In this work we characterize the CO emissions phenomenology in the DC/Baltimore area and quantify the absolute emissions and their temporal characteristics. We find that while the seasonal cycle appears modest, the monthly and annual variability is considerable and there is a clear Sunday effect in emissions. This result implies that emission estimates can benefit from continuous updating, especially during times of rapid changes in emission drivers, and that the temporal variability in CO emissions must be considered to better understand air quality in urban areas.

The US EPA National Emissions Inventory estimated trend based on bottom-up models agrees well with the results presented in this work (2015 – 2020) as well as with previous work<sup>3</sup> in the area (1997 – 2010). Together, these results highlight that more efficient combustion and emissions controls put in place by Federal and State Governments have been successful in achieving a long-term reduction in CO emissions. However, both our results and the EPA trends also suggest that in the last decade, CO emission reductions have slowed, which also has implications for trends of co-emitted mobile source VOCs and primary and secondary-forming PM<sub>2.5</sub> emissions.<sup>2,7</sup> Several metropolitan regions of the US still violate the ambient air quality standard for ozone and PM<sub>2.5</sub>, which impacts human health,<sup>58</sup> and continued emissions control may be needed to continue improving the air quality in our cities.

The anomaly in emissions due to the pandemic response, while substantial at 16 % (or

23 % depending on the reference) for April and May 2020, was only a transitory reduction mainly driven by a decline of  $\approx 35$  % in traffic. However, this decrease also offers a partial glimpse into the emissions reductions possibly achievable if  $\approx 35$  % of the combustion-powered vehicles were removed or replaced with non-emitting vehicles, assuming that the same composition of the fleet as that caused the reduction in traffic during the COVID period is maintained during the transition. We recognize, however that such a reduction (or more) could be achieved by targeting the high-emitting vehicles on the tail of the distribution.<sup>59,60</sup>

Future work is needed to better understand the seasonal cycle of CO as well as to monitor the impact on emissions as the fleet transitions to non-combustion engines by continuing to update the emissions in the study area in near real-time, as well as to compare to other cities with potentially different combinations of sources and degree of technology penetration. Additional pollutants and trace gases, like GHGs, should also be considered to increase our understanding of source composition and emission factors relative to CO<sub>2</sub>.

## Acknowledgement

Funding was provided by the National Institute of Standards and Technology Greenhouse Gas measurements program (awards 70NANB21H021, 70NANB16H262, 70NANB17H303, 70NANB19H037 and 70NANB19H167), National Oceanic and Atmospheric Administration AC4 program (NA14OAR0110139 / NA14OAR0110140), COVID-19 related funding from NOAA's Office of Ocean and Atmospheric Research (OAR), NOAA NRDD Project #19533 and the Maryland Department of Environment.

Certain commercial equipment, instruments, or materials are identified in this paper in order to specify the experimental procedure adequately. Such identification is not intended to imply recommendation or endorsement by the National Institute of Standards and Technology, nor is it intended to imply that the materials or equipment identified are necessarily the best available for the purpose.

## References

- (1) Hallock-Waters, K. A.; Doddridge, B. G.; Dickerson, R. R.; Spitzer, S.; Ray, J. D. Carbon monoxide in the U.S. mid-Atlantic troposphere: Evidence for a decreasing trend. *Geophysical Research Letters* **1999**, *26*, 2861–2864.
- (2) McDonald, B. C.; Gentner, D. R.; Goldstein, A. H.; Harley, R. A. Long-Term Trends in Motor Vehicle Emissions in U.S. Urban Areas. *Environmental Science & Technology* **2013**, *47*, 10022–10031.
- (3) He, H.; Stehr, J. W.; Hains, J. C.; Krask, D. J.; Doddridge, B. G.; Vinnikov, K. Y.; Canty, T. P.; Hosley, K. M.; Salawitch, R. J.; Worden, H. M.; Dickerson, R. R. Trends in emissions and concentrations of air pollutants in the lower troposphere in the Baltimore/Washington airshed from 1997 to 2011. *Atmospheric Chemistry and Physics* **2013**, *13*, 7859–7874.
- (4) Yin, Y.; Chevallier, F.; Ciais, P.; Broquet, G.; Fortems-Cheiney, A.; Pison, I.; Saunois, M. Decadal trends in global CO emissions as seen by MOPITT. *Atmospheric Chemistry and Physics* **2015**, *15*, 13433–13451.
- (5) Hedelius, J. K.; Toon, G. C.; Buchholz, R. R.; Iraci, L. T.; Podolske, J. R.; Roehl, C. M.; Wennberg, P. O.; Worden, H. M.; Wunch, D. Regional and Urban Column CO Trends and Anomalies as Observed by MOPITT Over 16 Years. *Journal of Geophysical Research: Atmospheres* **2021**, *126*.
- (6) Buchholz, R. R. et al. Air pollution trends measured from Terra: CO and AOD over industrial, fire-prone, and background regions. *Remote Sensing of Environment* **2021**, *256*, 112275.
- (7) McDonald, B. C.; Goldstein, A. H.; Harley, R. A. Long-Term Trends in California Mobile Source Emissions and Ambient Concentrations of Black Carbon and Organic Aerosol. *Environmental Science & Technology* **2015**, *49*, 5178–5188.

- (8) (EPA), E. P. A. *2017 National Emissions Inventory, Complete Release. Technical Support Document*; 2020.
- (9) Quéré, C. L.; Jackson, R. B.; Jones, M. W.; Smith, A. J. P.; Abernethy, S.; Andrew, R. M.; De-Gol, A. J.; Willis, D. R.; Shan, Y.; Canadell, J. G.; Friedlingstein, P.; Creutzig, F.; Peters, G. P. Temporary reduction in daily global CO<sub>2</sub> emissions during the COVID-19 forced confinement. *Nature Climate Change* **2020**, *10*, 647–653.
- (10) Forster, P. M.; Forster, H. I.; Evans, M. J.; Gidden, M. J.; Jones, C. D.; Keller, C. A.; Lamboll, R. D.; Quéré, C. L.; Rogelj, J.; Rosen, D.; Schleussner, C.-F.; Richardson, T. B.; Smith, C. J.; Turnock, S. T. Current and future global climate impacts resulting from COVID-19. *Nature Climate Change* **2020**, *10*, 913–919.
- (11) Liu, Z. et al. Near-real-time monitoring of global CO<sub>2</sub> emissions reveals the effects of the COVID-19 pandemic. *Nature Communications* **2020**, *11*.
- (12) McDonald, B. C.; McBride, Z. C.; Martin, E. W.; Harley, R. A. High-resolution mapping of motor vehicle carbon dioxide emissions. *Journal of Geophysical Research: Atmospheres* **2014**, *119*, 5283–5298.
- (13) Gately, C. K.; Hutyra, L. R.; Peterson, S.; Wing, I. S. Urban emissions hotspots: Quantifying vehicle congestion and air pollution using mobile phone GPS data. *Environmental Pollution* **2017**, *229*, 496–504.
- (14) McDonald, B. C. et al. Modeling Ozone in the Eastern U.S. using a Fuel-Based Mobile Source Emissions Inventory. *Environmental Science & Technology* **2018**, *52*, 7360–7370.
- (15) Gerbig, C.; Lin, J. C.; Wofsy, S. C.; Daube, B. C.; Andrews, A. E.; Stephens, B. B.; Bakwin, P. S.; Grainger, C. A. Toward constraining regional-scale fluxes of CO<sub>2</sub> with atmospheric observations over a continent: 2. Analysis of COBRA data using a receptor-oriented framework. *Journal of Geophysical Research: Atmospheres* **2003**, *108*, n/a–n/a.

- (16) Cui, Y. Y. et al. Top-down estimate of methane emissions in California using a mesoscale inverse modeling technique: The South Coast Air Basin. *Journal of Geophysical Research: Atmospheres* **2015**, *120*, 6698–6711.
- (17) Cui, Y. Y. et al. Top-down estimate of methane emissions in California using a mesoscale inverse modeling technique: The San Joaquin Valley. *Journal of Geophysical Research: Atmospheres* **2017**, *122*, 3686–3699.
- (18) Sheng, J.-X.; Jacob, D. J.; Turner, A. J.; Maasakkers, J. D.; Sulprizio, M. P.; Bloom, A. A.; Andrews, A. E.; Wunch, D. High-resolution inversion of methane emissions in the Southeast US using SEAC4RS aircraft observations of atmospheric methane: anthropogenic and wetland sources. *Atmospheric Chemistry and Physics* **2018**, *18*, 6483–6491.
- (19) Brioude, J.; Kim, S.-W.; Angevine, W. M.; Frost, G. J.; Lee, S.-H.; McKeen, S. A.; Trainer, M.; Fehsenfeld, F. C.; Holloway, J. S.; Ryerson, T. B.; Williams, E. J.; Petron, G.; Fast, J. D. Top-down estimate of anthropogenic emission inventories and their interannual variability in Houston using a mesoscale inverse modeling technique. *Journal of Geophysical Research* **2011**, *116*.
- (20) Brioude, J. et al. Top-down estimate of surface flux in the Los Angeles Basin using a mesoscale inverse modeling technique: assessing anthropogenic emissions of CO, NO and CO<sub>2</sub> and their impacts. *Atmospheric Chemistry and Physics* **2013**, *13*, 3661–3677.
- (21) Lopez-Coto, I.; Ren, X.; Salmon, O. E.; Karion, A.; Shepson, P. B.; Dickerson, R. R.; Stein, A.; Prasad, K.; Whetstone, J. R. Wintertime CO<sub>2</sub>, CH<sub>4</sub>, and CO Emissions Estimation for the Washington, DC–Baltimore Metropolitan Area Using an Inverse Modeling Technique. *Environmental Science & Technology* **2020**, *54*, 2606–2614.
- (22) Gourdji, S. M.; Yadav, V.; Karion, A.; Mueller, K. L.; Conley, S.; Ryerson, T.; Nehr Korn, T.; Kort, E. A. Reducing errors in aircraft atmospheric inversion estimates

of point-source emissions: the Aliso Canyon natural gas leak as a natural tracer experiment. *Environmental Research Letters* **2018**, *13*, 045003.

(23) Lopez-Coto, I.; Ghosh, S.; Prasad, K.; Whetstone, J. Tower-based greenhouse gas measurement network design—The National Institute of Standards and Technology North East Corridor Testbed. *Advances in Atmospheric Sciences* **2017**, *34*, 1095–1105.

(24) Karion, A.; Callahan, W.; Stock, M.; Prinzivalli, S.; Verhulst, K. R.; Kim, J.; Salameh, P. K.; Lopez-Coto, I.; Whetstone, J. Greenhouse gas observations from the Northeast Corridor tower network. *Earth System Science Data* **2020**, *12*, 699–717.

(25) Plant, G.; Kort, E. A.; Floerchinger, C.; Gvakharia, A.; Vimont, I.; Sweeney, C. Large Fugitive Methane Emissions From Urban Centers Along the U.S. East Coast. *Geophysical Research Letters* **2019**, *46*, 8500–8507.

(26) WMO, Carbon Monoxide (CO) WMO Scale, WMO-CO-X2014A. [https://gml.noaa.gov/ccl/co\\_scale.html](https://gml.noaa.gov/ccl/co_scale.html), 2018.

(27) Ren, X. et al. Methane Emissions From the Baltimore-Washington Area Based on Airborne Observations: Comparison to Emissions Inventories. *Journal of Geophysical Research: Atmospheres* **2018**, *123*, 8869–8882.

(28) Stein, A. F.; Draxler, R. R.; Rolph, G. D.; Stunder, B. J. B.; Cohen, M. D.; Ngan, F. NOAA’s HYSPLIT Atmospheric Transport and Dispersion Modeling System. *Bulletin of the American Meteorological Society* **2015**, *96*, 2059–2077.

(29) (NOAA-ARL), A. R. L. NAM12: North American Mesoscale Forecast System. <ftp://arlftp.arlhq.noaa.gov/pub/archives/nam12>, 2020.

(30) Hersbach, H. et al. The ERA5 global reanalysis. *Quarterly Journal of the Royal Meteorological Society* **2020**, *146*, 1999–2049.

- (31) (C3S), C. C. C. S. ERA5: Fifth generation of ECMWF atmospheric reanalyses of the global climate. <https://cds.climate.copernicus.eu/cdsapp#!/home>, 2017.
- (32) Lin, J. C. A near-field tool for simulating the upstream influence of atmospheric observations: The Stochastic Time-Inverted Lagrangian Transport (STILT) model. *Journal of Geophysical Research* **2003**, *108*, ACH 2–1–ACH 2–17.
- (33) Loughner, C. P.; Fasoli, B.; Stein, A. F.; Lin, J. C. Incorporating features from the Stochastic Time-Inverted Lagrangian Transport (STILT) model into the Hybrid Single-Particle Lagrangian Integrated Trajectory (HYSPLIT) model: a unified dispersion model for time-forward and time-reversed applications. *Journal of Applied Meteorology and Climatology* **2021**,
- (34) Rödenbeck, C.; Gerbig, C.; Trusilova, K.; Heimann, M. A two-step scheme for high-resolution regional atmospheric trace gas inversions based on independent models. *Atmospheric Chemistry and Physics* **2009**, *9*, 5331–5342.
- (35) Enting, I. *Inverse Problems in Atmospheric Constituent Transport*; Cambridge Atmospheric and Space Science Series; Cambridge University Press, 2002.
- (36) Tarantola, A.; for Industrial, S.; Mathematics, A. *Inverse Problem Theory and Methods for Model Parameter Estimation*; Other titles in applied mathematics; Society for Industrial and Applied Mathematics, 2005.
- (37) Michalak, A. M. A geostatistical approach to surface flux estimation of atmospheric trace gases. *Journal of Geophysical Research* **2004**, *109*.
- (38) Andres, R. J.; Boden, T. A.; Higdon, D. M. Gridded uncertainty in fossil fuel carbon dioxide emission maps, a CDIAC example. *Atmospheric Chemistry and Physics* **2016**, *16*, 14979–14995.



- (39) Gately, C. K.; Hutyra, L. R. Large Uncertainties in Urban-Scale Carbon Emissions. *Journal of Geophysical Research: Atmospheres* **2017**, *122*, 11,242–11,260.
- (40) Gourdj, S. M.; Hirsch, A. I.; Mueller, K. L.; Yadav, V.; Andrews, A. E.; Michalak, A. M. Regional-scale geostatistical inverse modeling of North American CO<sub>2</sub> fluxes: a synthetic data study. *Atmospheric Chemistry and Physics* **2010**, *10*, 6151–6167.
- (41) Engelen, R. J. On error estimation in atmospheric CO<sub>2</sub> inversions. *Journal of Geophysical Research* **2002**, *107*.
- (42) Desroziers, G.; Berre, L.; Chapnik, B.; Poli, P. Diagnosis of observation, background and analysis-error statistics in observation space. *Quarterly Journal of the Royal Meteorological Society* **2005**, *131*, 3385–3396.
- (43) Shusterman, A. A.; Kim, J.; Lieschke, K. J.; Newman, C.; Wooldridge, P. J.; Cohen, R. C. Observing local CO<sub>2</sub> sources using low-cost, near-surface urban monitors. *Atmospheric Chemistry and Physics* **2018**, *18*, 13773–13785.
- (44) Turner, A.; Kim, J.; Fitzmaurice, H.; Newman, C.; Worthington, K.; Chan, K.; Wooldridge, P.; Köhler, P.; Frankenberg, C.; Cohen, R. C. Observed impacts of COVID-19 on urban CO<sub>2</sub> emissions. *Earth and Space Science Open Archive* **2020**, *9*.
- (45) McDonald, B. C. WRF-Chem emissions inventory for CONUS and Eastern US domains for NY-ICE/LISTOS 2018 modeling. <https://csl.noaa.gov/groups/csl17/measurements/mobilelab/MobileLabNYICE/DataDownload/wrfchem.php>, 2018.
- (46) (EPA), E. P. A. EPA Air Pollutant Emissions Trends Data. [https://www.epa.gov/sites/production/files/2018-07/state\\_tier1\\_caps.xlsx](https://www.epa.gov/sites/production/files/2018-07/state_tier1_caps.xlsx), 2018.
- (47) FHWA, Travel Monitoring Analysis System. <https://www.fhwa.dot.gov/policyinformation/tables/tmasdata/>, 2018.

- 482 (48) FHWA, Travel Monitoring Analysis System. [https://www.fhwa.dot.gov/](https://www.fhwa.dot.gov/policyinformation/tables/tmasdata/)  
483 [policyinformation/tables/tmasdata/](https://www.fhwa.dot.gov/policyinformation/tables/tmasdata/), 2019.
- 484 (49) FHWA, Travel Monitoring Analysis System. [https://www.fhwa.dot.gov/](https://www.fhwa.dot.gov/policyinformation/tables/tmasdata/)  
485 [policyinformation/tables/tmasdata/](https://www.fhwa.dot.gov/policyinformation/tables/tmasdata/), 2020.
- 486 (50) Apple, Apple Mobility Trends Reports. <https://covid19.apple.com/mobility>, 2020.
- 487 (51) EIA, EIA Monthly, state-level “Prime Supplier Sales Volumes” for “motor gasoline” for  
488 DC. [https://www.eia.gov/dnav/pet/pet\\_sum\\_mkt\\_dcu\\_sDC\\_m.htm](https://www.eia.gov/dnav/pet/pet_sum_mkt_dcu_sDC_m.htm), 2020.
- 489 (52) EIA, EIA Monthly, state-level “Prime Supplier Sales Volumes” for “motor gasoline” for  
490 Maryland. [https://www.eia.gov/dnav/pet/pet\\_sum\\_mkt\\_dcu\\_SMD\\_m.htm](https://www.eia.gov/dnav/pet/pet_sum_mkt_dcu_SMD_m.htm), 2020.
- 491 (53) EIA, EIA Monthly, state-level “Prime Supplier Sales Volumes” for “motor gasoline” for  
492 Virginia. [https://www.eia.gov/dnav/pet/pet\\_sum\\_mkt\\_dcu\\_sVA\\_m.htm](https://www.eia.gov/dnav/pet/pet_sum_mkt_dcu_sVA_m.htm), 2020.
- 493 (54) Warneke, C.; de Gouw, J. A.; Holloway, J. S.; Peischl, J.; Ryerson, T. B.; Atlas, E.;  
494 Blake, D.; Trainer, M.; Parrish, D. D. Multiyear trends in volatile organic compounds  
495 in Los Angeles, California: Five decades of decreasing emissions. *Journal of Geophysical*  
496 *Research: Atmospheres* **2012**, *117*, n/a–n/a.
- 497 (55) Bishop, G. A.; Haugen, M. J. The Story of Ever Diminishing Vehicle Tailpipe Emissions  
498 as Observed in the Chicago, Illinois Area. *Environmental Science & Technology* **2018**,  
499 *52*, 7587–7593.
- 500 (56) Jiang, Z.; McDonald, B. C.; Worden, H.; Worden, J. R.; Miyazaki, K.; Qu, Z.;  
501 Henze, D. K.; Jones, D. B. A.; Arellano, A. F.; Fischer, E. V.; Zhu, L.; Boersma, K. F.  
502 Unexpected slowdown of US pollutant emission reduction in the past decade. *Proceed-*  
503 *ings of the National Academy of Sciences* **2018**, *115*, 5099–5104.
- 504 (57) Nisbet, E.; Weiss, R. Top-Down Versus Bottom-Up. *Science* **2010**, *328*, 1241–1243.

- 505 (58) Di, Q.; Wang, Y.; Zanobetti, A.; Wang, Y.; Koutrakis, P.; Choirat, C.; Dominici, F.;  
506 Schwartz, J. D. Air Pollution and Mortality in the Medicare Population. *New England*  
507 *Journal of Medicine* **2017**, *376*, 2513–2522.
- 508 (59) Bishop, G. A.; Schuchmann, B. G.; Stedman, D. H.; Lawson, D. R. Multispecies remote  
509 sensing measurements of vehicle emissions on Sherman Way in Van Nuys, California.  
510 *Journal of the Air & Waste Management Association* **2012**, *62*, 1127–1133.
- 511 (60) Winkler, S. L.; Anderson, J. E.; Garza, L.; Ruona, W. C.; Vogt, R.; Wallington, T. J.  
512 Vehicle criteria pollutant (PM, NO<sub>x</sub>, CO, HCs) emissions: how low should we go? *npj*  
513 *Climate and Atmospheric Science* **2018**, *1*, 1–5.

514      **Graphical TOC Entry**

515

